Design and Performance Evaluation of LH_2 Cooling System for HTS Motor Electric Propulsion Platform

Kihwan Kim, Seongyong Hahn, Byungho Min, Ki-Deok Sim, and Seokho Kim

***Abstract*—This study focuses on developing an electric propulsion platform that utilizes liquid hydrogen (LH_2) as both fuel and coolant. The cooling system aims to cryogenically cool the rotor of a high-temperature superconductor (HTS) motor with LH_2 while supplying the discharged hydrogen to the fuel cell. By omitting an additional cryocooler for the HTS motor, this approach enhances efficiency and overall performance. The research includes the thermohydraulic and structural design of the HTS magnet rotor, incorporating LH_2 and a triple tube-magnetic fluid seal. A prototype cooling system was fabricated, and its performance evaluated using liquid nitrogen (LN_2) as an alternative refrigerant to ensure safety. LN_2 verified the flow and boiling heat transfer characteristics of the HTS rotor cooling system, with the flow rate controlled by the pressure build-up (PBU) method in the LN_2 vessel, relying on ambient heat load.**

***Index Terms*—Cooling system, cryogenic rotary coupling, HTS magnets, liquid hydrogen, magnet cooling, motors, PBU method, pressure control, propulsion, superconducting and system integration, transportation.**

I. Introduction

CURRENT researches focuses on hydrogen as a sustainable energy source for fuel cell electric propulsion systems.[1], [2], [3] To improve energy density and reduce operational pressure, cryogenic liquid hydrogen (LH_2) is proposed as an alternative, stored at pressures below 5 bar for lower energy consumption during injection and discharge. For power generation, LH_2 must convert to gaseous H_2 at room temperature via heat exchange. Research is also underway to replace conventional motors with high-temperature superconducting (HTS) motors, which require cryogenic cooling. Previous studies using cryocoolers and circulating components faced challenges such as capacity limitations, weight, and power losses.[4], [5], [6], [7] This study proposes a system linking HTS motors with LH_2 fuel cell power generation, utilizing LN_2 to cool the rotating rotor and HTS field coil while supplying the fuel cell. A test device was fabricated to evaluate these characteristics. The proposed cooling system features rotary seals and multilayer concentric tubes for the HTS rotor. LH_2 transfer utilizes the natural external heat load of the vessel and a pressure control valve via the PBU method, allowing LH_2 use without extra power. Operational conditions for the HTS rotor ensure safety during testing with LN_2.

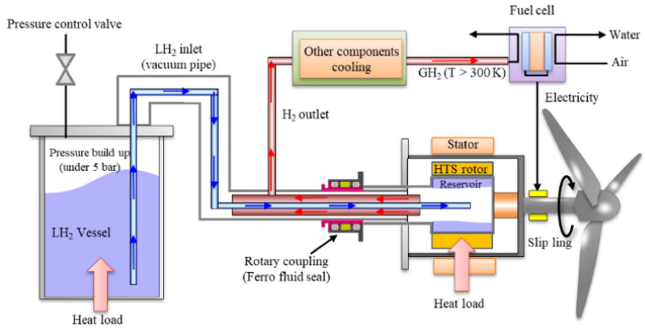

Fig. 1. LH_2-HTS motor electric propulsion system diagram.

II. System Topology and Thermal Design

A. System Topology and Conditions Define

The cooling and fuel supply system is illustrated in Fig. 1, with the flow path comprising the LH_2 vessel, HTS motor, and fuel cell. LH_2 cools the rotor during transfer and is also utilized for power generation. Each component is designed according to its specific role and operating conditions. In Fig. 1, the field coil employs a partial HTS motor. The layout modifies previous designs and enhances fluid transfer methods. The system operates at a pressure range of 1 to 3 bar, supplying LH_2 to the HTS motor through a multilayer concentric tube with a rotary joint for boiling cooling. After cooling the HTS motor, the discharged H_2 is directed to the fuel cell. If necessary, additional cooling via heat exchange occurs before supplying gaseous H_2 at temperatures above room temperature to the fuel cell. The operating conditions of key components are detailed in Table I [8].

Received 25 September 2024; revised 24 December 2024; accepted 3 January 2025. Date of publication 14 January 2025; date of current version 14 February 2025. This work was supported in part by the National R&D Program through the National Research Foundation of Korea (NRF), in part by the Ministry of Science, and in part by ICT under Grant 2022M3I9A1073187 and Grant 2019R1A5A8083201. *(Corresponding author: Seokho Kim.)*

Kihwan Kim is with the Department of Smart Manufacturing Engineering, Changwon National University, Changwon 51140, South Korea (e-mail: kkhtoo89@gmail.com).

Seongyong Hahn is with Seoul National University, Seoul 08826, South Korea (e-mail: hahnsy@snu.ac.kr).

Byungho Min is with Hyundai Motor Company, Uiwang-si 16082, South Korea (e-mail: mbh8994@hyundai.com).

Ki-Deok Sim is with SuperGenics Company Ltd, Changwon 51543, South Korea (e-mail: skedy@supergenics.co.kr).

Seokho Kim is with the Department of Mechanical Engineering, Changwon National University, Changwon-si 51140, South Korea (e-mail: seokho@changwon.ac.kr).

Color versions of one or more figures in this article are available at https://doi.org/10.1109/TASC.2025.3529421.

Digital Object Identifier 10.1109/TASC.2025.3529421

TABLE I
DEFINE OPERATING CONDITION OF SYSTEM

Component	Parameter	Unit	Value
LH_2 vessel	Operating pressure	bar	1~3
	LH_2 temperature (@ sat.)	K	20.4~22.9
	Latent heat (@ 1.4 g/s)	W	726~702
	Supply method		PBU method
HTS motor	Rated motor power	kW	100
	Operating Temperature	K	30
	Operating current	A	278
	Rotation speed range	RPM	100~800
	Motor heat load	W	Stationary : 31.8 Operating : 57.7
Fuel cell	Fuel cell output power	kW	100
	Fuel cell efficiency	%	50
	Need to LH_2	g/s	1.4 g/s

B. Cooling Relationship Between LH_2 Supply and Heat Load

This study proposes system that uses LH_2 as both coolant for the HTS motor and fuel for the fuel cell. Typically, mobility applications utilize proton exchange membrane fuel cells (PEMFCs) with an efficiency of around 50%. [9], [10]

The power generated by the PEMFC must exceed the HTS motor's required power output, determining the LH_2 flow rate. The flow rate for the fuel cell can be calculated as follows [11], [12]:

$$\dot{m}_{LH_2} = 1.05 \times 10^{-8} \times \frac{P_e}{V_c} \tag{1}$$

A critical aspect of the proposed system is ensuring the flow rate needed for fuel cell power generation is adequate for cooling the motor. Assuming a motor output of 100 kW and a fuel cell efficiency of 50%, the required LH_2 flow rate is approximately 1.4 g/s. At this flow rate, the achievable cooling capacity through latent heat is 726 W at a minimum pressure of 1 bar and 702 W at a maximum pressure of 3 bar. Given that the rated operating temperature of the HTS rotor is approximately 30 K and the assumed heat load is 60 W, sufficient cooling can be achieved with about 9% of the fuel cell supply flow rate. In conclusion, the H_2 discharged while cooling the HTS rotor is expected to be primarily in a saturated liquid state, with some portion in a saturated gas state, representing an ideal fluid. Since the fuel cell requires gaseous H_2 at temperatures above room temperature, the discharged LH_2 can also cool the armature coil, inverter, and fuel cell.

C. HTS Rotor Thermal Design

The position and size of the magnets are determined, creating spaces that necessitate a supporting structure to hold the coils and transmit rotational torque. To achieve initial cooling and maintain the operating temperature of the HTS rotor, heat exchange with LH_2 in a vacuum-insulated container is essential. Fig. 2 illustrates the shape of the HTS rotor, which includes a polygonal chamber (reservoir) made of highly conductive metal at the center of the HTS field coil, with a multilayer concentric tube inserted. This design allows LH_2 to perform boiling heat

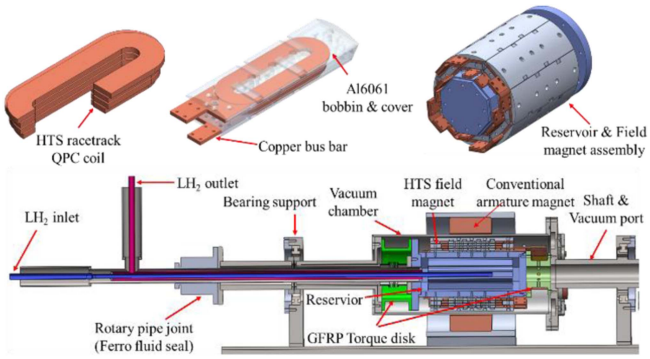

Fig. 2. HTS motor and LH_2 cooling system modeling.

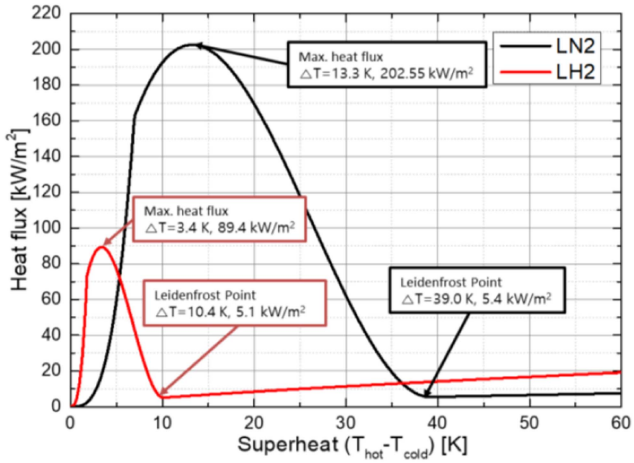

Fig. 3. Boiling curve of LN_2 and LH_2.

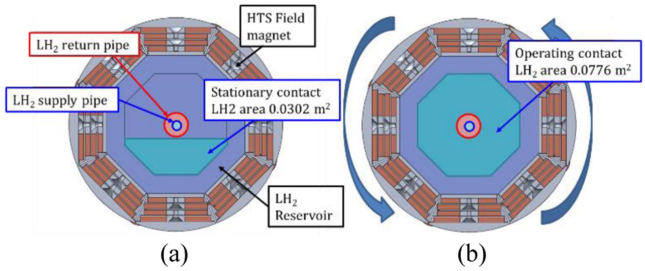

Fig. 4. LH_2 position in reservoir (a) stationary (b) operating.

transfer within the reservoir, cooling the HTS field coil attached to its exterior surface. A critical aspect of the cooling mechanism is whether initial cooling and temperature maintenance during rated operation can be achieved with a supply flow rate of 1.4 g/s. Although the latent heat is calculated to be sufficient compared to the motor's heat load, it is important to assess the internal boiling area of the reservoir based on the boiling curve of LH_2. The boiling curve and heat transfer amount of the cryogenic fluid are calculated as shown in Fig. 3. Fig. 4 illustrates the contact area considering the distribution of LH_2 within the reservoir during stationary and operational phases.[13] The heat loads during initial cooling and operational states are assumed to be 31.8 W and 57.7 W, respectively. Given the expected contact areas of

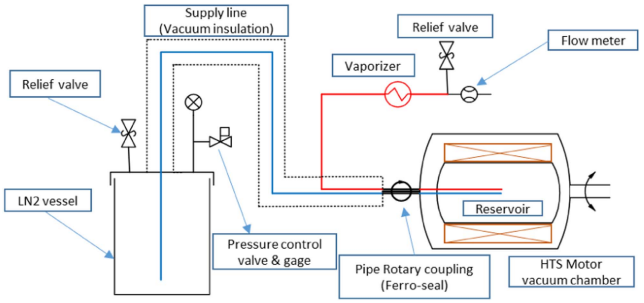

Fig. 5. Test device configuration P&ID.

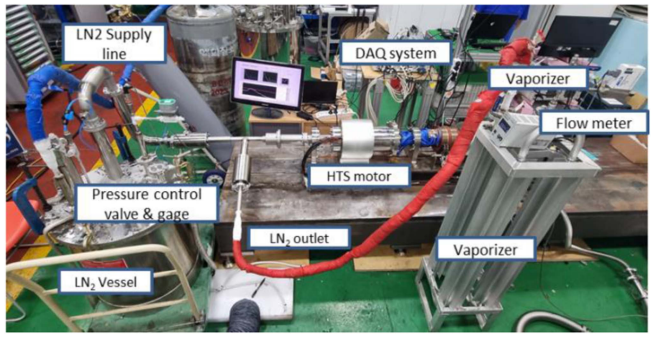

Fig. 6. Test device set up configuration.

0.0302 m^2 and 0.0776 m^2, the calculated heat fluxes by HTS rotor heat load are 1.05 kW/m^2 at stationary and 0.74 kW/m^2 at operating, which are lower than the Leidenfrost point shown in Figs. 3 and 4, indicating that stable cooling is achievable

D. LH_2 Vessel and Flow Supply Through PBU Method

The LH_2 vessel is designed to store LH_2 and maintain a pressure range of 1 to 3 bar. Cryogenic fluid storage typically encounters external heat loads, even with vacuum insulation. Inside the LH_2 vessel, LH_2 exists in a saturated state at the internal pressure when not injected in a sub-cooled condition. Consequently, evaporation occurs due to external heat, leading to increased internal pressure. This pressure rise also elevates the saturation temperature of LH_2, impeding effective storage and cooling. However, controlling the vessel's natural pressure increase below a certain level using a pressure control valve during LH_2 transfer allows for maintaining a low saturation temperature and internal pressure. The PBU method for fluid transfer offers the advantage of operating without additional devices like pumps or blowers, thus avoiding increased weight and power loss. In the proposed LH_2-HTS motor electric propulsion platform, the pressure and saturation temperature of the LH_2 vessel are determined by:

$$T_{LH2} \propto P_{vessel} \tag{2}$$

$$P_{vessel} = P_{atm} + \triangle P_{line} \tag{3}$$

The internal pressure of the LH_2 vessel equals the sum of pressure losses in the flow path when supplying the required flow rate. To maintain the operating temperature of the HTS motor that needs cooling, lowering the vessel operating pressure is advantageous for reducing the saturation temperature of LH_2. Therefore, the system designer must consider pressure losses in the supplied flow rate to optimize the temperature of the refrigerant transferred from the vessel.

III. Device Composition and Similarity Test

A. Similarity Test Design and Setup

The test was designed and fabricated to include supply lines and components, excluding the fuel cell, as shown in Fig. 5 . To ensure safety during tests and prevent explosions, a cryogenic fluid was needed to replace LH_2. In this study, liquid nitrogen (LN_2) was used as the test fluid due to its low flammability and toxicity. Pressure generation for LN_2 transfer was achieved using natural external thermal loads, and a pressure control valve was implemented to maintain a constant flow rate through PID control. All piping and components supplying fluid from the vessel to the HTS rotor were equipped with vacuum insulation to minimize phase change during transfer. The piping system featured a rotary coupling structure with a ferrofluid seal for connection to the HTS rotor. [14], [15] To simulate the cooling of the HTS rotor and the subsequent cooling of other components with a two-phase fluid before supplying it to the fuel cell at room temperature, a vaporizer was installed. A mass flow meter was placed at the final outlet to measure the flow rate. To validate the design and demonstrate the system's feasibility, the test device focused on three key areas:

1) A rotary coupling for LH_2 transport and vacuum insulation at high speeds
2) Maintaining a constant flow rate from the LH_2 vessel
3) Achieving and maintaining the HTS rotor's cooling temperature during operation

The flow rate was controlled at 1.4 g/s, referencing the calculated mass flow rate of LH_2 from initial cooling to the end of operation. The operational status of the rotary coupling was simulated by mounting a separate motor outside the HTS rotor and adjusting the RPM to mimic mechanical drive. To simulate the heat generation occurring when current is applied to the HTS magnet, a 15 W output heater was installed on the coil cover to replicate the operational thermal load.

IV. Test Results and Analysis

In the test results, the vessel pressure was maintained at 1.45 bar to supply a constant flow rate of 1.4 g/s. Initial cooling took 2 hours, during which the temperature of the HTS magnet ranged from a maximum of 83 K to a minimum of 80.5 K. This indicates that the temperature difference between the HTS magnet and LH_2 was 2 K. When applying LH_2, considering the material properties of the reservoir and coil bobbin, the temperature difference is anticipated to increase by a factor of 2.5, resulting in 4.5 K. [16] Therefore, it can be predicted that the temperature of the HTS magnet will reach 24.5 K when supplied with LH_2 at 20 K. The highest temperature was observed at the HTS magnet connected to the external current leads, attributed

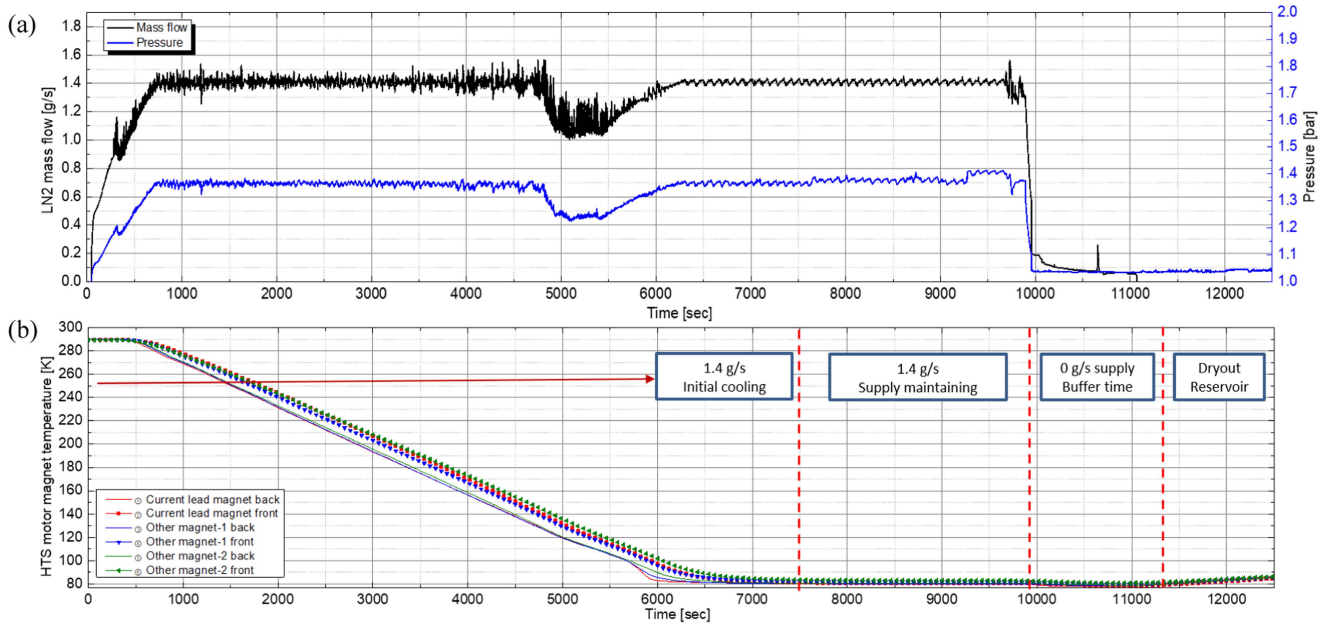

Fig. 7. Initial cooling results (a) mass flow rate and LN_2 vessel pressure (b) HTS dummy coil temperature.

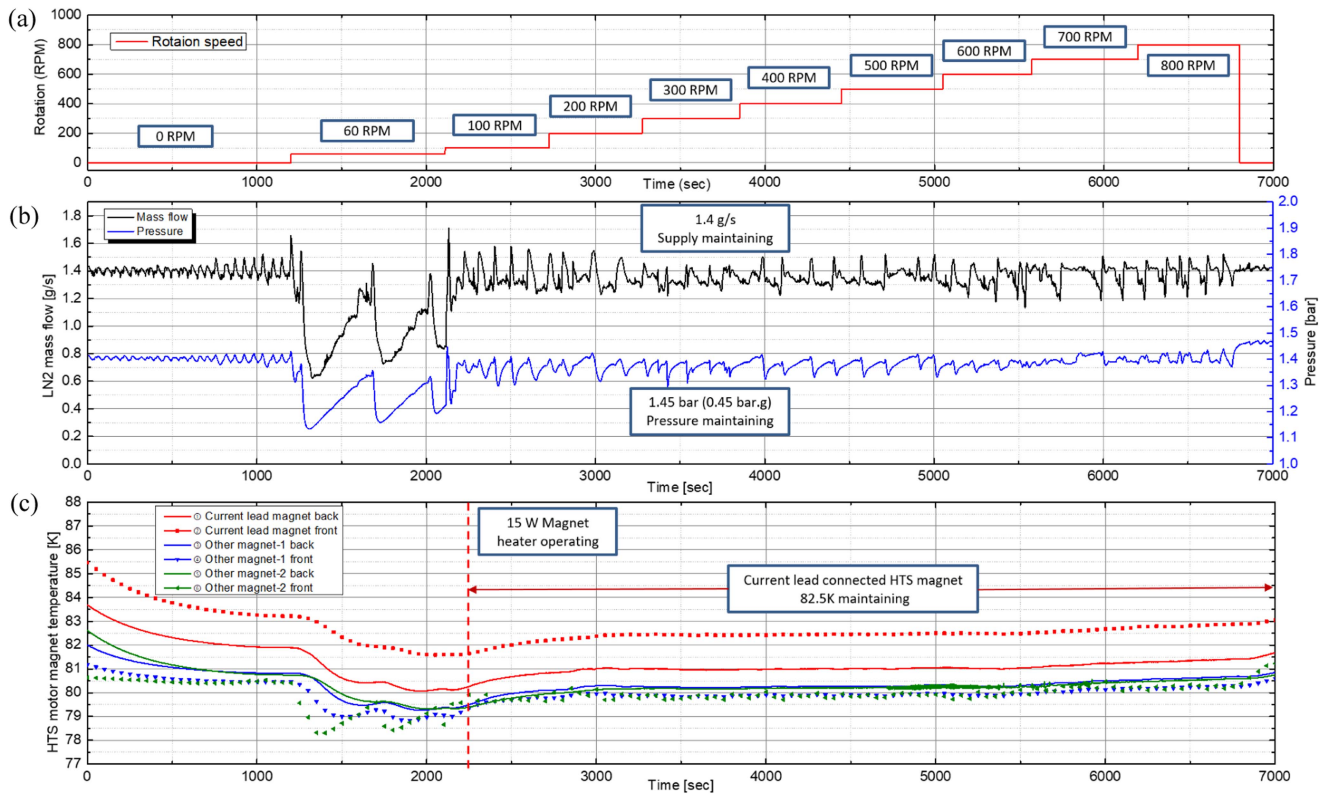

Fig. 8. Test results of rotational drive (a) RPM change (b) mass flow rate and LN2 vessel pressure (c) HTS dummy coil temperature.

to conductive heat ingress. A temporary decrease in pressure and flow at the 5000-second mark was analyzed as a rapid boiling phase change due to the reservoir temperature crossing the Leidenfrost point, as shown in Fig. 3. [17], [18] After halting LN_2 supply, the remaining LN_2 in the reservoir maintained the cooling temperature for about 20 minutes before rising to a dry-out condition. In rotational tests simulating HTS motor operation, the system was driven at 60 RPM and then sustained at 100 to 800 RPM for 10 minutes each. At 60 RPM, the temperature and flow were unstable due to insufficient centrifugal force

causing oscillation of LN_2 in the reservoir, hindering effective PID control of the pressure control valve. Stability was regained at 100 RPM, maintaining consistent cooling temperature and flow until reaching 800 RPM. Throughout the tests, the cooling temperatures of all electromagnets decreased by approximately 1 K compared to initial cooling, attributed to increased heat flux as LN_2 distributed under centrifugal force, as shown in Fig. 4(b). Overall, the results indicate that stable cooling of the HTS rotor is achievable when supplying a consistent flow rate for the fuel cell during both initial cooling and operational states.

V. Conclusion

This study presents the design of a HTS motor electric propulsion platform that utilizes LH_2 as both a refrigerant and a fuel, alongside the development of a similarity testing setup. Performance assessment through cryogenic testing with LN_2 demonstrated the system's capability to maintain a consistent flow during both initial cooling and operational conditions within the HTS motor temperature range. The results confirm the feasibility of an integrated system that links an LH_2 storage vessel, the HTS motor, and a fuel cell, thereby eliminating the need for separate cryogenic cooling and refrigerant supply systems. Future work will focus on evaluating the performance of the HTS motor using LH_2.

References

[1] A. Hoffrichter, S. Hillmansen, and C. Roberts, "Conceptual propulsion system design for a hydrogen-powered regional train," *IET Elect. Syst. Transp.*, vol. 6, no. 2, pp. 56–66, 2016.

[2] J. K. Nøland, R. Mellerud, and C. Hartmann, "Next-generation cryo-electric hydrogen-powered aviation: A disruptive superconducting propulsion system cooled by onboard cryogenic fuels," *IEEE Ind. Electron. Mag.*, vol. 16, no. 4, pp. 6–15, Dec. 2022, doi: 10.1109/MIE.2022.3174332.

[3] N. Shakeri, M. Zadeh, and J. B. Nielsen, "Hydrogen fuel cells for ship electric propulsion: Moving toward greener ships," *IEEE Electrific. Mag.*, vol. 8, no. 2, pp. 27–43, Jun. 2020, doi: 10.1109/mele.2020.2985484.

[4] D. Silva, F. Ferreira, J. F. P. Fernandes, and P. J. D. C. Branco, "Barriers and challenges going from conventional to cryogenic superconducting propulsion for hybrid and all-electric aircrafts," *Energies*, vol. 14, 2021, Art. no. 6861, doi: 10.3390/en14216861.

[5] G.-D. Nam, L. D. Vuong, H.-J. Sung, S. J. Lee, and M. Park, "Conceptual design of an aviation propulsion system using hydrogen fuel cell and superconducting motor," *IEEE Trans. Appl. Supercond.*, vol. 31, no. 5, Aug. 2021, Art. no. 5202307, doi: 10.1109/TASC.2021.3064526.

[6] D. S. Dezhin and I. N. Dezhina, "Development of the future aircraft propulsion system based on HTS electrical equipment with liquid hydrogen cooling," *IEEE Trans. Appl. Supercond.*, vol. 32, no. 4, Jun. 2022, Art. no. 3601105, doi: 10.1109/TASC.2022.3153246.

[7] D. Dezhin, I. Dezhina, and R. Ilyasov, "Superconducting propulsion system with LH2 cooling for all-electric aircraft," *J. Phys., Conf. Ser.*, vol. 1559, Jun. 2020, Art. no. 012143, doi: 10.1088/1742-6596/1559/1/012143.

[8] K. Kim, S. Hahn, B. Min, K.-D. Sim, Y. Kim, and S. Kim, "Liquid hydrogen cooling system for 100 kW-class HTS rotor thermal design," *IEEE Trans. Appl. Supercond.*, vol. 34, no. 5, Aug. 2024, Art. no. 5202305, doi: 10.1109/TASC.2024.3366151.

[9] R. E. Rosli et al., "A review of high-temperature proton exchange membrane fuel cell (HT-PEMFC) system," *Int. J. Hydrogen Energy*, vol. 42, no. 14, pp. 9293–9314, Apr. 2017, doi: 10.1016/j.ijhydene.2016.06.211.

[10] A. Dicks and D. A. J. Rand, *Fuel Cell Syst. Explained*, 3rd ed.. Hoboken, NJ, USA: Wiley, 2018, pp. 405–409, doi: 10.1002/9781118706992.

[11] A. L. Dicks and D. A. J. Rand, "Appendix 2: Useful fuel-cell equations," in *Fuel Cell Systems Explained*, A. L. Dicks and D. A. J. Rand, Eds., 2018, doi: 10.1002/9781118706992.app2.

[12] A. Kabza, "Fuel cell formulary," Pemfc.de, Accessed: Dec. 25, 2024. [Online]. Available: https://www.pemfc.de/FCF_Smart.pdf

[13] J. Kim, D. Kwon, and S. Jeong, "Conceptual design of hybrid electric vertical take-off and landing (eVTOL) aircraft with a liquid hydrogen fuel tank," *Prog. Supercond. Cryogenics*, vol. 24, no. 2, pp. 27–38, Jun. 2022, doi: 10.9714/PSAC.2022.24.2.027.

[14] B. Felder, M. Miki, K. Tsuzuki, R. Sato, H. Hayakawa, and M. Izumi, "Cryogenic rotary joints applied to the cooling of superconducting rotating machinery," *IEEE Trans. Appl. Supercond.*, vol. 23, no. 3, Jun. 2013, Art. no. 5201204, doi: 10.1109/TASC.2013.2241382.

[15] R. Sato, B. Felder, M. Miki, K. Tsuzuki, H. Hayakawa, and M. Izumi, "Helium-neon gas mixture thermosyphon cooling and stability for large scale HTS synchronous motors," *IEEE Trans. Appl. Supercond.*, vol. 23, no. 3, Jun. 2013, Art. no. 5200704, doi: 10.1109/TASC.2013.2241592.

[16] "Cryogenic material properties 6063-T5 aluminum," Nist.gov, Accessed: Dec. 25, 2024. [Online]. Available: https://trc.nist.gov/cryogenics/materials/6063_T5%20Alulminum/6063-T5Aluminum_rev.htm

[17] R. F. Barron and G. F. Nellis. *Cryogenic Heat Transfer*, 2nd ed.. Boca Raton, FL, USA: CRC Press, 2016, pp. 142–147, doi: 10.1201/b20225.

[18] L. Wang, Y. Li, F. Zhang, F. Xie, and Y. Ma, "Correlations for calculating heat transfer of hydrogen pool boiling," *Int. J. Hydrogen Energy*, vol. 41, no. 38, pp. 17118–17131, 2016, doi: 10.1016/j.ijhydene.2016.06.254.